PAPER • OPEN ACCESS

Enhanced electrochemical performance of solution-processed single-wall carbon nanotube reinforced polyvinyl alcohol nanocomposite synthesized via solution-cast method

View the article online for updates and enhancements.

NANO EXPRESS

PAPER

Enhanced electrochemical performance of solution-processed single-wall carbon nanotube reinforced polyvinyl alcohol nanocomposite synthesized via solution-cast method

Muhammad Rakibul Islam[1] , S M Nazmus Shakib Pias[1], Rabeya Binta Alam[1] and Saiful I Khondaker[2,3]

[1] Department of Physics, Bangladesh University of Engineering and Technology (BUET), Dhaka, Bangladesh
[2] Department of Physics, University of Central Florida, Orlando, FL-32826, United States of America
[3] NanoScience Technology Center, University of Central Florida, Orlando, FL-32826, United States of America

E-mail: rakibul@phy.buet.ac.bd

Abstract

Polyvinyl alcohol/surfactant-free single-walled carbon nanotube (PVA/SF-SWNT) nanocomposites were synthesized by a facile solution-cast technique. The effect of SF-SWNT on the structural, surface-morphological, mechanical, electrical, and electrochemical properties of the nanocomposite was studied. The surface morphology and Fourier Transform Infrared Spectroscopy demonstrate an increased degree of interaction between PVA and SF-SWNT resulting in improved mechanical strength of the nanocomposite. Incorporation of SF-SWNT was found to improve the DC electrical conductivity by almost five orders of magnitude. Furthermore, the effect of SWNT on the electrochemical properties of the nanocomposite was also studied. The PVA/SF-SWNT composite exhibits specific capacitance as high as $26.4 \, \text{F g}^{-1}$ at a current density $0.5 \, \text{mA g}^{-1}$, which is four times higher than that of PVA ($6.1 \, \text{F g}^{-1}$). The impedance spectroscopy analysis reveals that the incorporation of SWNT reduces the charge transfer resistance of the nanocomposites resulting in better capacitive performance.

1. Introduction

In recent years, polymer-based nanocomposite has gained significant attention both from research as well as from the application point of view. Incorporation of nano-sized filler into the polymer matrix widen the area of applications by modifying the physiochemical properties of the composite. The easy processability, improved mechanical properties together with resistant against harsh environment allows polymer nanocomposite to replace the conventional materials and are used in a number of versatile applications, including food packaging, nanosensors, fuel cell, battery electrodes, supercapacitors, etc [1–5]. Various nanostructured materials such as nanoparticles, carbon nanotubes (CNT), graphene, etc have been used as nanofillers for the polymer nanocomposite [4–8]. Among them, CNT with extraordinary mechanical strength, high thermal stability, and electrical conductivities make them the best alternatives as a filler [9–12].

Synthesis of high-quality polymer nanocomposite with the optimum performance required a homogeneous dispersion of carbon nanotube within the polymer matrix [13, 14]. However, the inherent attractive van der walls interaction between nanotubes causes agglomerations of CNTs, which significantly decreases the overall surface area of CNTs when exposed to the surrounding polymer matrix that severely affects the performance of the nanocomposite [15, 16]. An attractive and well-established way to get rid of the agglomeration of CNTs is to use surfactant. The surfactants coat a layer on the CNT surface that allows them to keep separated and promotes homogeneous dispersion of CNTs in the polymer matrix [17]. A major drawback of this method is that the surfactant residue may present at the CNT surface and cannot be removed completely which degrade the properties of the CNT based nanocomposite [18]. The use of surfactant-free SWNT can offer a remedy to this

problem. Surfactant free SWNTs (SF-SWNTs) are defect-free, clean, non-agglomerated, and offer enabling route for the synthesis of different functional devices such as FET, SETs, sensors, supercapacitors, etc [19–23]. Mostly, solution-processed SF-SWNTs were used for the synthesis of functional devices and their performance has been evaluated. However, there exist very few reports on the effect of SF-SWNT on polymer nanocomposite. So a comprehensive study is therefore required to understand the effect of surfactant-free SWNT on polymer nanocomposite.

The objective of the present work is to study the effect of SF-SWNT on polymer nanocomposite. Poly (vinyl alcohol) (PVA), one of the most widely used synthetic polymers was used as the matrix. Due to its easy processability, and low cost together with excellent chemical resistance and physical properties PVA found a broad range of applications in the automotive, textile, and packaging industries [24]. In most of the published article CNT powder were used to make CNT solution with which PVA was mixed to make the nanocomposite. However, to the best of our knowledge solution-processed SWNT was never used to make PVA-based CNT nanocomposite. The synthesis method plays a key role in controlling the surface morphology, structural and optical properties of the nanocomposite. Several methods are being adapted for the synthesis of carbon nanotubes based polymer nanocomposites, which include *in situ* polymerization, melt mixing, melt intercalation, solution casting, etc. Among them, the solution casting method is a versatile, rapid, simple, and economic process for the synthesis of polymer nanocomposite. Due to these advantages, the cost-efficient solution cast method has chosen for the synthesis of PVA/SF-SWNT nanocomposite and their structural, surface morphological, electrical, mechanical, and electrochemical properties have been reported in this article.

2. Materials and methods

2.1. Materials
Polyvinyl alcohol (PVA) with an average molecular weight of $\sim$125,000 g mol^{-1} (98% hydrolyzed) was obtained from Sigma-Aldrich. A stable, surfactant-free solution of SWNTs with a concentration of SWNTs $\sim$50 μg ml^{-1} was purchased from Brewer Science. The original solution was then diluted using de-ionized (DI) water to obtain the desired concentration. The solution consists of mostly individual SWNTs and is free of catalytic particles [20, 21]. All chemicals were used as received and without purifications.
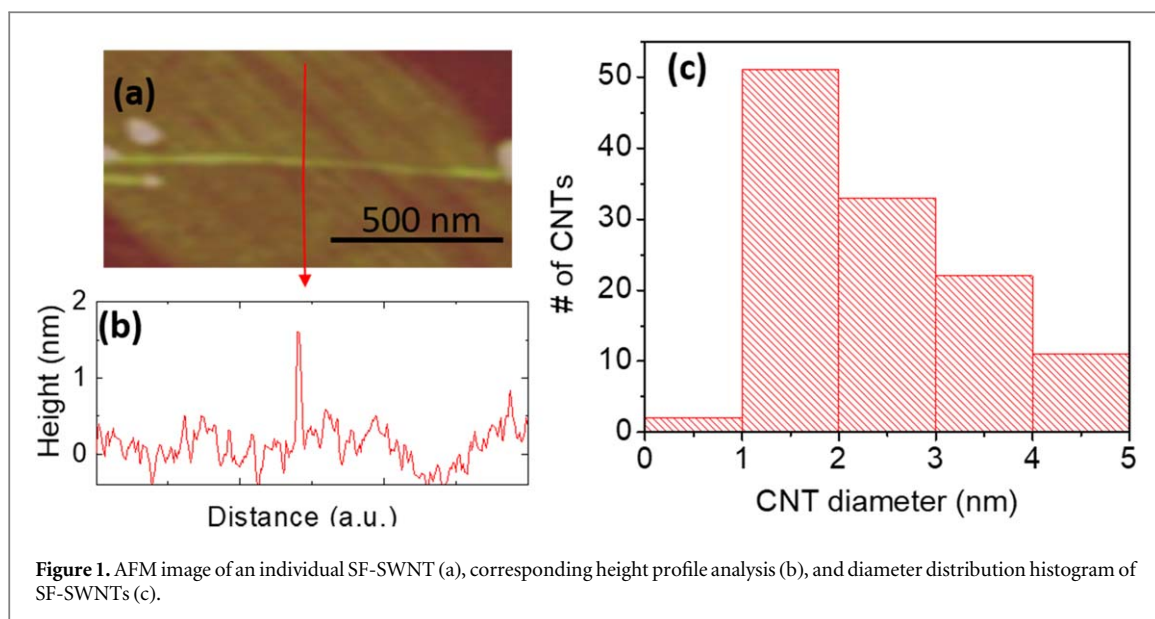
2.2. Sample preparation
First, PVA (1 g) was dissolved in 50 ml of DI water and heated at 70 °C for 30 min to fully dissolve the solute. The solution was then cooled to room temperature and ultrasonicated for 1 h. For the synthesis of nanocomposite high-quality well-dispersed SWNT solution was gradually added to the PVA solution and heated under continuous stirring until the solution became viscous. The viscous solution was ultrasonicated for 1 h and then poured into a Polytetrafluoroethylene (PTFE) coated pan. The as-cast solution was then dried in an oven for 24 h to obtain a thin film of PVA/SF-SWNT nanocomposite. A schematic for the synthesis of the PVA/SF-SWNT nanocomposite method was presented in the supplementary figure S1 is available online at stacks.iop.org/ NANOX/1/030013/mmedia. Different volume (0 μl, 100 μl, 200 μl, and 400 μl) of SF-SWNTs solutions were added to the PVA samples and the resultant PVA/SF-SWNT nanocomposite were named as sample A, Sample B, Sample C, and Sample D respectively.

2.3. Characterization of PVA/SF-SWNT nanocomposite
AFM images were taken on a Dimension 3100 scanning probe microscope (Vecco Instruments Inc.) to study the diameter distribution of the SF-SWNTs. For the AFM study, the SF-SWNT suspension was spin-coated on a mica substrate. Images were obtained using tapping mode and collected under ambient conditions at 60% relative humidity and at 27 °C with a scanning rate of 0.6 Hz. For AFM imaging, tip-shaped silicon nitride probes with a tip radius of 2 nm were used. Figure 1(a) displays a tapping-mode AFM image of a single SF-SWNT. Figure 1(b) shows the height analysis of the corresponding SF-SWNT. Figure 1(c) shows the diameter distributions of a number of SF-SWNT. The bar diagram shows that the diameter of the solution-processed SWNT varies between 0.5 nm–5.0 nm with an average diameter of 1.5 nm.

The presence of different groups in the nanocomposites was studied by Fourier transform infrared spectroscopy (FTIR) analysis. The chemical analysis by FTIR in attenuated total reflection (ATR) mode was carried out using a (Shimadzu IRSpirit) spectrophotometer at a spectrum range of 640–4000 cm^{-1}.

The Young modulus, tensile strength, elongation at break, ductility, and toughness of the samples were measured on a universal testing machine (Wance ETM 501), maximum capacity 50 KN) at room temperature with gauge length 5 mm, width 20 mm, and thickness less than 0.2 mm, and a crosshead speed of 10 mm min^{-1}. The standard test method for tensile properties of thin plastic sheeting (specification ASTM D882-02) was followed. An average value of five replicates for each sample was taken for the tensile tests.

Figure 1. AFM image of an individual SF-SWNT (a), corresponding height profile analysis (b), and diameter distribution histogram of SF-SWNTs (c).

After the tensile test, the fractured surface of the PVA and PVA/SF-SWNT was observed using a field emission scanning electron microscope (JEOL JSM-7600F) at an accelerating voltage of 5 kV. Prior to imaging, the samples were sputtered with a thin layer of gold.

The thermal properties of PVA/SF-SWNT nanocomposites were studied by differential scanning calorimetric (DSC) analysis. For DSC, the samples were heated from 25 °C to 250 °C. Each time the samples were heated at a rate of 10 °C min^{-1} and were kept in a nitrogen atmosphere at a flow rate of 40 ml min^{-1} to avoid thermo-oxidative degradation.

The DC electrical properties of the nanocomposite were studied by a homemade four-point collinear probe setup featuring gold-coated spring-loaded pins.

Cyclic voltammetry (CV), galvanostatic charge-discharge measurements (GCD), and electrochemical impedance analysis (EIS) were carried out with a CS310 electrochemical workstation (corrtest, china). The electrochemical measurements were carried out in a conventional three-electrode cell setup: glassy carbon electrode with electro-active material (1 mg) as the working electrode, platinum plate (1 × 1 cm^2) as the counter electrode, Ag/AgCl reference electrode was used as the reference electrode and 0.1 M KCl solution was used as the electrolyte.

3. Results and discussion

3.1. FTIR Analysis of PVA/SF-SWNT nanocomposite
The FTIR spectra of pure PVA and PVA/SF-SWNT composites were presented in figure 2. For pure PVA a broad peak was observed between 3050 cm^{-1} to 3650 cm^{-1}, centered at 3295 cm^{-1}. This can be attributed to the symmetric stretching vibrations of the O–H from the intramolecular and intermolecular hydrogen bonds [25, 26]. The band centered at 2915 cm^{-1} arises from the symmetric and antisymmetric stretching vibration of the C–H alkyl group. The band at 1733 cm^{-1} can be attributed to the stretching vibration mode of the C=O bond. The peak observed at 1374 cm^{-1} corresponds to the wagging vibration mode of the CH$_2$ group. The peak at 1243 cm^{-1} can be attributed to the combination of the C–H wagging vibration mode and the C–O stretching mode of the acetyl groups [27, 28]. It was also observed that the incorporation of SF-SWNT shifts the position of the O–H stretching peak to a lower wavenumber in the nanocomposite. This suggests the presence of hydrogen bonding interactions between the hydroxyl groups on the PVA molecular chains of the nanocomposite. The shift towards lower frequency may be due to the open of p-bonds of SWNTs and interactions between SWNTs and the PVA matrix. Moreover, the intensity of the O–H stretching band at 3050 cm^{-1} to 3650 cm^{-1} shows a decreasing pattern with the incorporation of SWNT. Such a reduction in intensity might be attributed to the partial removal of the OH groups in the PVA matrix due to the incorporation of SWNT [29].

3.2. Surface morphology of PVA/SF-SWNT nanocomposite
The SEM images of the fractured surfaces of the PVA/SF-SWNT composites were shown in figure 3. The cross-section of the nanocomposites looked smooth, and no residual structure of SWNT was observed for the nanocomposite. Similar morphological behavior was also observed for PVA based carbon nanotube composite
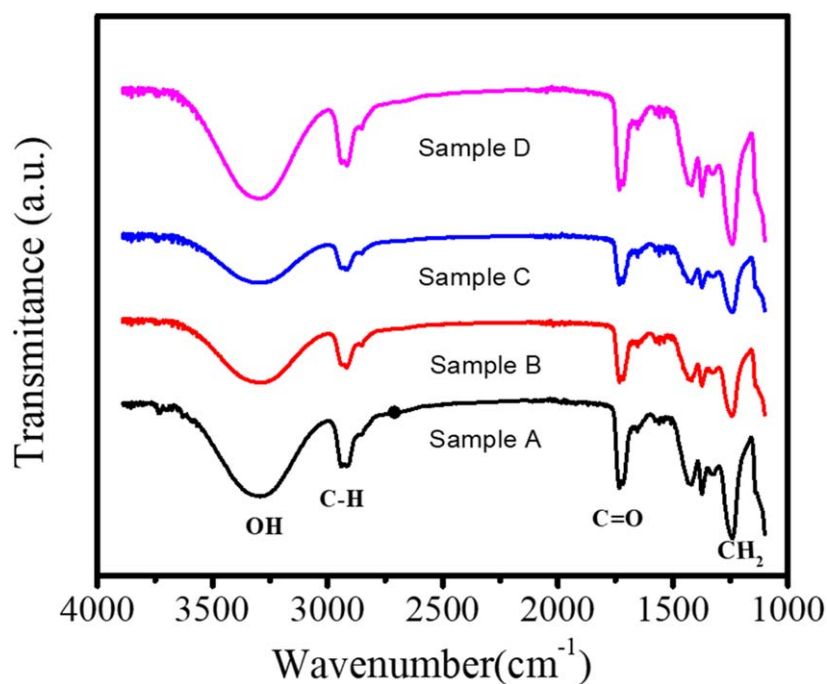
Figure 2. FTIR spectra of PVA/SF-SWNT nanocomposites with different concentrations of SWNT.
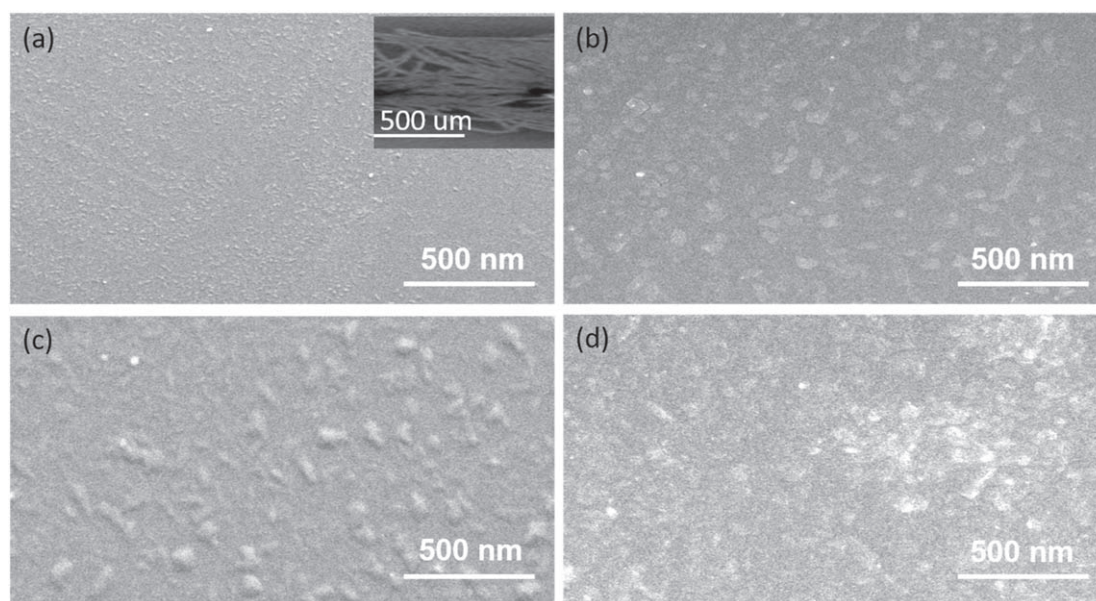

Figure 3. SEM micrographs of different PVA/SF-SWNT nanocomposites (a) sample A, (b) Sample B, (c) Sample C, and (d) Sample D. Inset (a) shows the FESEM images of SF-SWNT.

film and can be attributed to the strong interfacial interactions between SWNT and the PVA matrix [30, 31]. Additionally, the roughness of the nanocomposite increases with the concentration of SWNT.

3.3. Thermal properties of PVA/SF-SWNT nanocomposite

Differential Scanning Calorimetry (DSC) technique was used to study the thermal transitions properties of the nanocomposite. DSC provides information about the glass transition temperature (T_g), melting temperature (T_m), and the degree of crystallinity (χ_c) of the material. Figure 4 shows the DSC curves for pure PVA and PVA/SF-SWNT nanocomposite. From the figure, it was observed that the glass transition occurs at around 50 °C for PVA and it decreases with the increase of SWNTs, indicating good interaction between PVA and SF-SWNT. Additionally, low glass transition temperature leads to the higher segmental motion of the polymer electrolyte
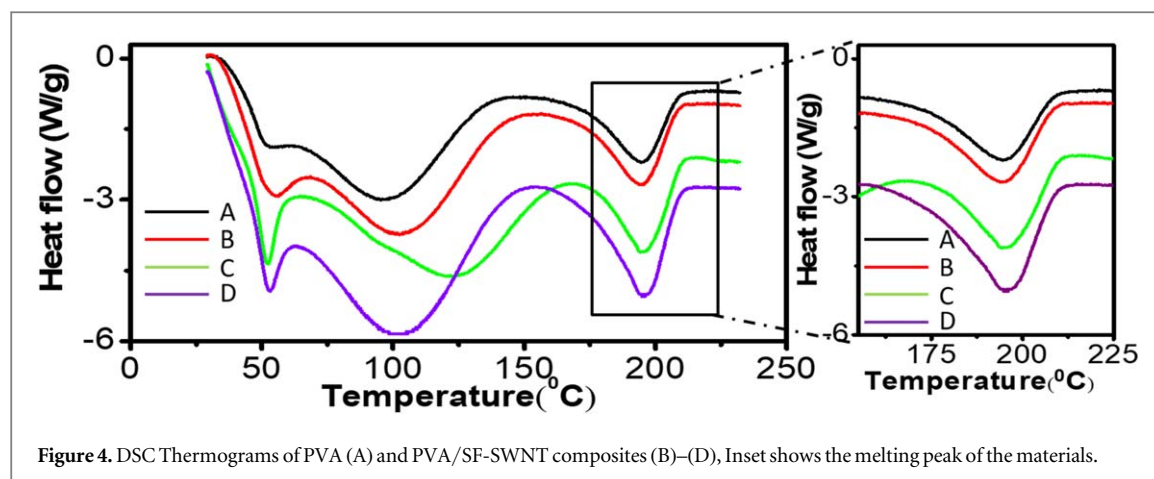
Figure 4. DSC Thermograms of PVA (A) and PVA/SF-SWNT composites (B)–(D), Inset shows the melting peak of the materials.

Table 1. Crystallinity (χ_c), specific capacitance (C_S), power density (P), and energy density (E) of PVA/SF-SWNTs nanocomposite.

Sample	SF-SWNT concentration per gram (μl)	Crystallinity χ_c (%)	Specific capacitance (C_S) (F g^{-1})	Power density (P) (W m^{-3})	Energy density (E) (Wh kg^{-1})
A	0	22.25	6.05	0.68	42.21
B	50	24.45	14.30	1.61	44.77
C	100	33.50	19.90	2.24	44.92
D	200	38.90	26.40	2.97	44.94

resulting in easy movement of ions through the polymer chain and ionic conductivity [25]. The observed peak around 150 °C corresponds to the vaporization of water contents in the polymer nanocomposite. Large endothermic peaks were observed between 170 °C–220 °C that corresponds to the melting of polymer nanocomposite. The relative percentage of crystallinity (%χ_c) was estimated from the melting peak using the formula [32].
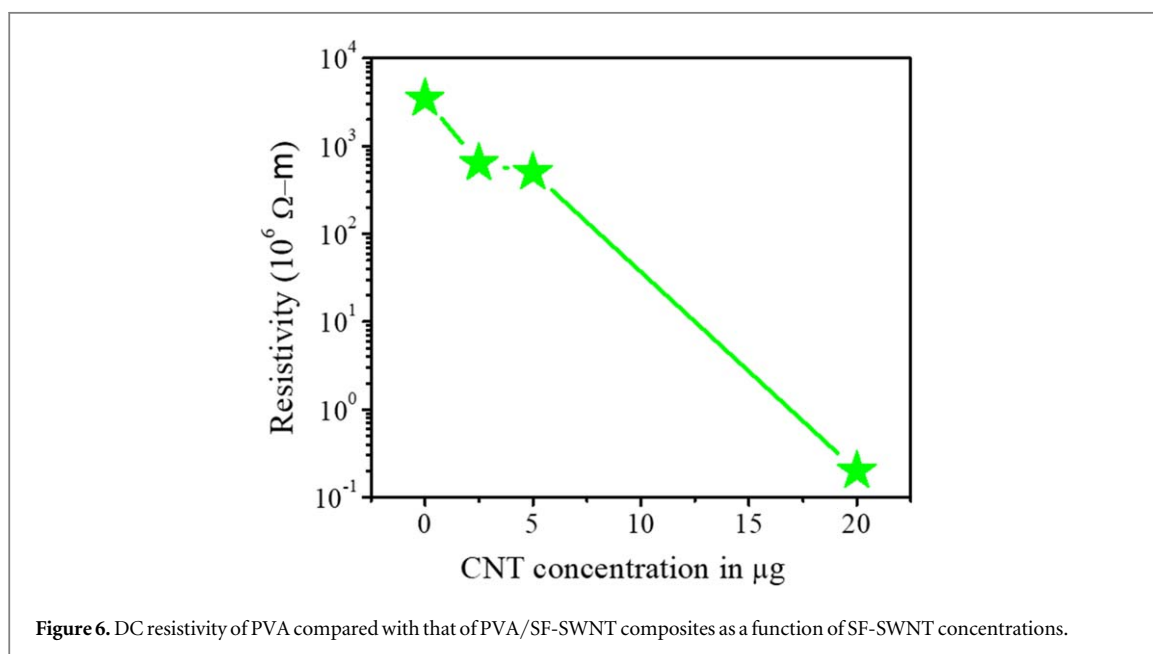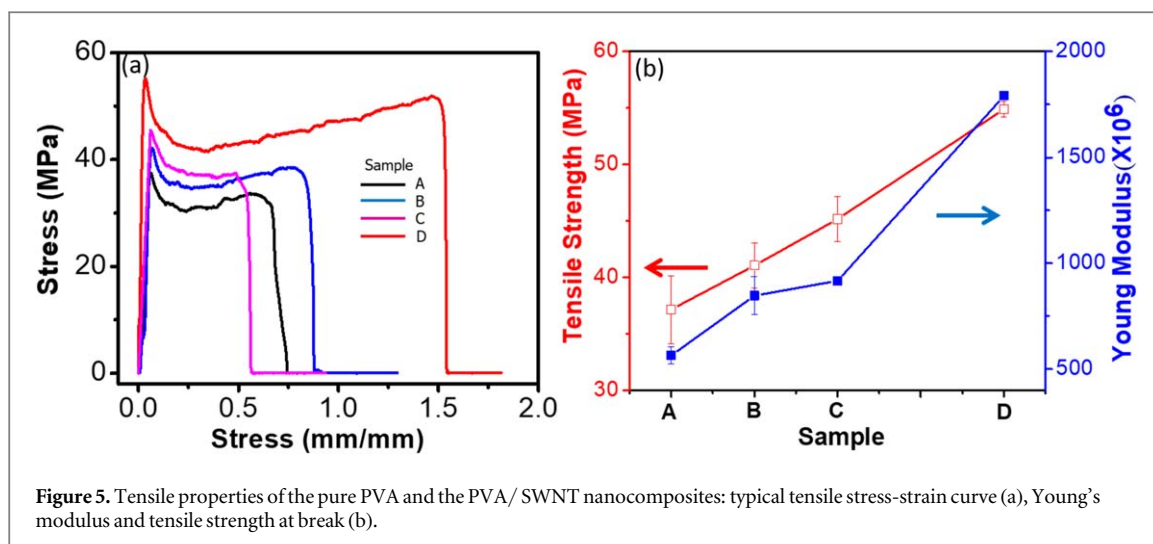
$$\%\chi_c = \frac{\Delta H_m}{\Delta H_m^0}$$

Where ΔH_m^0 is the melting enthalpy of pure PVA and ΔH_m is the melting enthalpy of PVA/SF-SWNT nanocomposite. The relative percentage of crystallinity (%χ_c) are listed in table 1. The crystallinity of the nanocomposite increased from 22% to 39% with the incorporation of SF-SWNT. This suggests that the SF-SWNT act as nucleation sites for the crystallization of PVA. Furthermore, the linear increase in crystallinity with the amount of SWNTs suggests that the SWNTs are surrounded by a crystalline coating of polymer around them [33]. These crystalline coating helps to improve the mechanical properties of the polymer nanocomposite by improving the stress transfer.

3.4. Mechanical properties of PVA/SF-SWNT nanocomposite

Tensile testing was performed to evaluate the effect of solution-processed SWNT on the mechanical properties of the PVA/SF-SWNT nanocomposite. Typical stress-strain curves for PVA and PVA/SF-SWNT nanocomposites for various concentrations of SWNTs were presented in figure 5(a). The addition of SWNT in the PVA matrix was found to increase the tensile strength of the composite and the tensile strength was increased by 50% (from 37 MPa to 55 MPa) for sample D. The result shows that incorporation of SF-SWNT significantly improved the mechanical performance of PVA films. As shown in figure 5(b), Young's modulus of the PVA/SF-SWNT nanocomposite was increased by almost three times for sample D.

The uniformity of the carbon nanotube dispersion in the polymer matrix and stronger polymer–nanotube interaction play a crucial role in the mechanical properties of the polymer–nanotube composite. Since the solution-processed SF-SWNTs were well dispersed in the solvent as well as to the polymer matrix, resulting in a significant increase in the tensile strength and tensile modulus. Furthermore, the aspect ratio of the solution-processed SWNT (with diameter ~2 nm) was high compared to that of the MWNT, bundled MWNTs, or bundled SWNTs [34, 35]. The large aspect ratio offers increased availability of the SWNT surface area to the surrounding polymer matrix that helps to increase the tensile stress transfer across the PVA/SF-SWNT interface [35].

Figure 5. Tensile properties of the pure PVA and the PVA/ SWNT nanocomposites: typical tensile stress-strain curve (a), Young's modulus and tensile strength at break (b).

Figure 6. DC resistivity of PVA compared with that of PVA/SF-SWNT composites as a function of SF-SWNT concentrations.

Additionally, the reinforcement of the nanotube/polymer composite depends on the total nanotube surface area per unit volume. In other words, keeping the concentration the same, nanotube with the larger surface area will provide superior mechanical performance, which in turn depends on the diameter of the nanotube [35, 36]. The increased surface area provided by the small diameter (~2 nm) SF-SWNT used in this study resulting in better tensile mechanical properties.

3.5. DC electrical properties of PVA/SF-SWNT nanocomposite

The electrical properties of the nanocomposite were studied by Van der Pauw four-point collinear probe methods. The resistivity, ρ of the thin films were calculated using the formula $\rho = 2\pi s(V/I)$ [37]. Where V is the potential difference between the inner probes in volt, I is the current through the outer pair of probes in ampere, S is the spacing between the probes in meter. Figure 6 showed the variation in the electrical resistivity of the nanocomposites as a function of the SWNT filler loading. A five-fold decrease in the electrical resistivity was observed when the concentration SF-SWNT was increased from 0 to 400 μl. The increase in conductivity with SWNT content signifies a typical percolation transition behavior. Since the electrical conductivity showed a four-fold increase when the concentration of SWNT increased from 5 μg ml^{-1} to 20 ug ml^{-1}, we can assume that the percolation occurred at an SWNT concentration of 20 ug ml^{-1}. The dispersion state of the filler is governed by a number of factors such as the structure of filler, rheological properties of the polymer matrix, polymer-filler compatibility, and mixing technique [38]. Additionally, for a particular polymer, the conductivity of the SWNT based nanocomposite depends strongly on the good dispersion of SWNTs, fabrication parameters,

Figure 7. Cyclic voltammograms of PVA (a), PVA/SF-SWNT 50 μl (b), 100 μl (c), and 200 μl (d), at different scan rates in 0.1 M KCl aqueous electrolyte for the potential window of 0.2 V to 0.7 V.
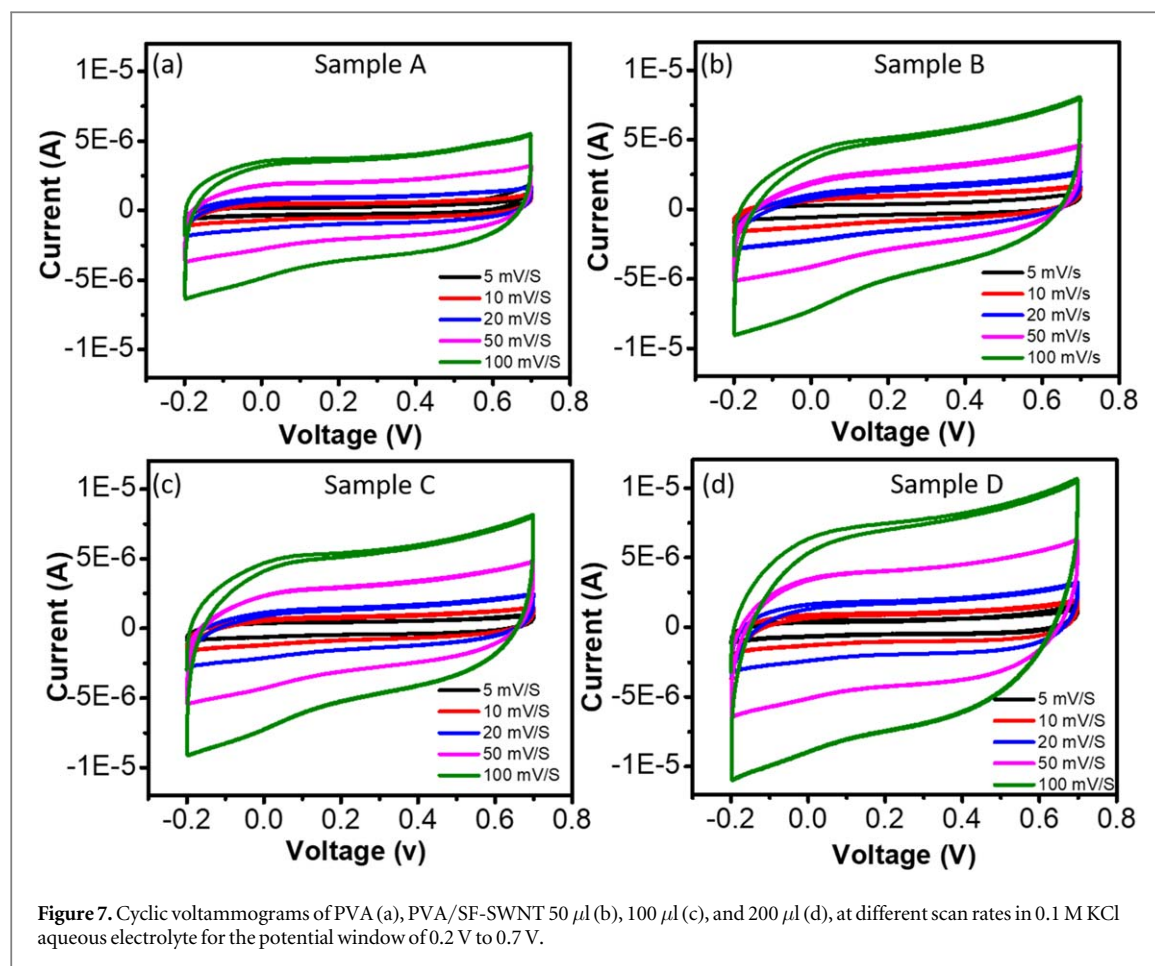
the aspect ratio of CNTs, the uniform spatial distribution of individual CNTs, and degree of alignment, etc The higher surface area of SWNTs offers a uniform distribution along with the PVA matrix as well as boosts the connection of fillers between each other; therefore, the increase in electrical properties was achieved. Moreover, with the higher SWNT loading, SWNTs were more strongly aligned by the inter-tube hydrogen-bonding interaction between the hydroxyl groups of the PVA-water solution resulting in a higher conduction path [39].

3.6. Electrochemical properties of PVA/SF-SWNT nanocomposite

To explore the effect of SF-SWNT on the capacitive behavior of the nanocomposite cyclic voltammograms (CV) were recorded. CV measurements were performed at different sweep rates namely, 5 mVs^{-1}, 10 mVs^{-1}, 20 mVs^{-1}, 50 mVs^{-1}, and 100 mVs^{-1} using 0.1 M KCL as the electrolyte in a potential window of 1 V and are presented in figure 7. The CV curves for PVA were found to be nearly rectangular for all scan rates. A distorted rectangular shape in the CV curve was observed for the PVA/SF-SWNT nanocomposite. Such a deviation from the rectangular shape can be attributed to the presence of pseudocapacitance originating from the presence of uncompensated resistance due to SWNTs present in the system [40]. Additionally, the cyclic voltammograms for the nanocomposite exhibit a sharp rise in current at a low voltage that drops sharply at the vertex potential indicating the good electrochemical stability of the electrode material. Figure 8 (a) shows the CV measurements for PVA and PVA/SF-SWNT for different nanotube loading at a scan rate of 100 mVs^{-1}. Notably, the quasi-rectangle area of CV curves of PVA/SF-SWNT was larger than that of pure PVA, indicating the better capacitive performance of PVA/SF-SWNT composites. Furthermore, the area of the CV curves increases with the amount of SF-SWNT nanofiller in the composite which implied that SWNT played key roles in speeding up carriers' transportation along the PVA networking chains.

Figure 8(b) shows the galvanostatic charge-discharge (GCD) curves of PVA and PVA/SF-SWNT nanocomposite at a constant current density of 0.5 mA cm^{-2}. The discharging curve of the nanocomposite shows two voltage ranges, a short discharge occurred between 0.7 V to 0.4 V which can be attributed to the electric double-layer capacitance originating from the charge separation at the electrode-electrolyte interface. A longer discharge occurred between 0.4 V to 0.1 V, which may be due to the combined effect of electric double-layer capacitance and the Faradaic capacitance [41]. From the figure, it was also observed that the discharging
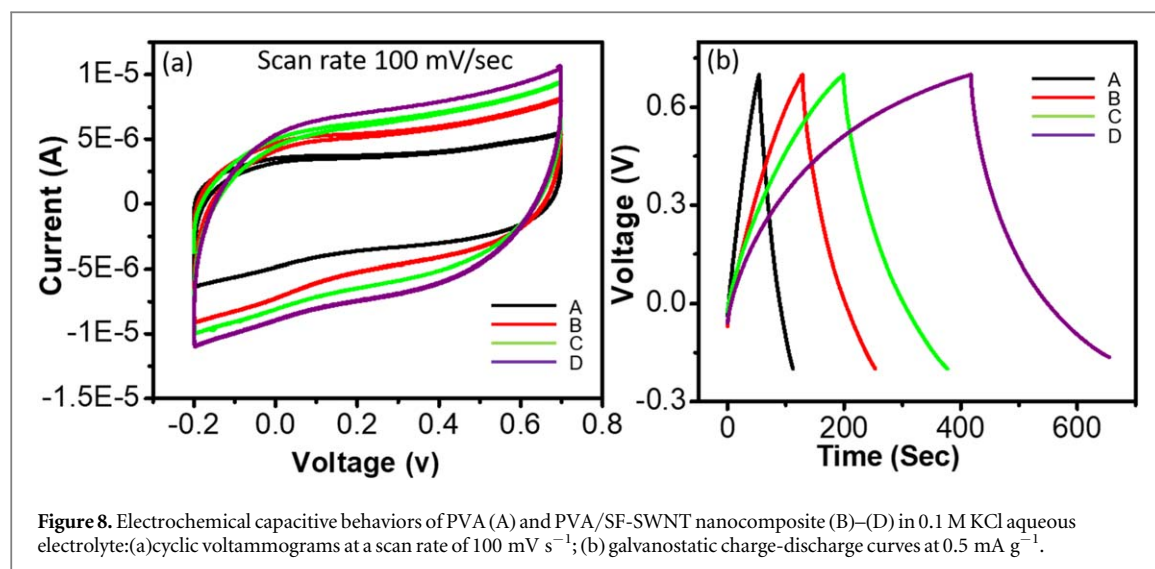
Figure 8. Electrochemical capacitive behaviors of PVA (A) and PVA/SF-SWNT nanocomposite (B)–(D) in 0.1 M KCl aqueous electrolyte:(a)cyclic voltammograms at a scan rate of 100 mV s^{-1}; (b) galvanostatic charge-discharge curves at 0.5 mA g^{-1}.

time of the composite increases with the concentration of SF-SWNT, suggesting improvement of the capacitive behavior of the materials.

The specific capacitances of the nanocomposites were estimated from their respective GCD curve using the formula $C_s = I\Delta t/m\Delta V$ [42]. Where, *I, t, V*, and *m* are the constant current (A), discharge time (s), total potential deviation (V), and the mass of the active materials within the electrode (g), respectively. All the specific capacitance data of these composites at different current densities were summarized in table 1. From table 1 it was clear that SF-SWNT significantly enhanced the capacitance of the nanocomposite. For example, for sample D, incorporation of just 0.002 wt% of SWNT enhances the specific capacitance by four times. The values of specific capacitances obtained in this study are higher compared to the specific capacitance reported earlier for solution-processed nanotube-based polymer composite [43–46]. For conducting PVA/CNT nanofibers specific capacitance as high as 25 F g^{-1} was obtained for 6 wt% CNT concentrations [47]. Even though specific capacitance higher than this study were reported for CNT based polymer nanocomposite but the concentration of CNTs used in these studies was few orders of magnitude higher than the present studies [48].

Such an enhancement in the specific capacitance of the nanocomposite can be attributed to a number of factors. Firstly, the quality of the SWNT: high-quality surfactant-free well-dispersed SWNT solution was used. The well-dispersed SWNTs with higher specific surface area increases the effective interfacial area between the nanocomposite and electrolyte that improves the specific capacitance by increasing the electroactive region [16]. Additionally, the presence of surfactant on the SWNT surface may diminish the gravimetric performance of the nanocomposite and reduces the non-Faradic ion storage behavior on SWNT surface sites [49, 50]. The absence of surfactant allows more SWNT to come to the nanotube surface and thereby enhance the capacitive performance. The energy density (E) and power density (P) of the nanocomposites were also measured using the formulas [51]

$$\text{Energy density,} \quad E = \frac{0.5 * (\Delta V)^2 * Cs}{3.6}$$

$$\text{Power density,} \quad P = \frac{E * 3600}{\Delta t}$$

The corresponding values of the *E* and *P* for different concentrations of SF-SWNT in the nanocomposites were presented in table 1. The energy and power density was also found to follow the same variations as that of the specific capacitance.

3.7. Impedance spectroscopy analysis

The electrochemical impedance spectroscopy (EIS) is an important characterization tool to evaluate the resistive behavior of the electrode. Figure 9 showed the respective Nyquist plots for PVA/SF-SWNT nanocomposite between 100 Hz to 1 MHz, where Z′ is the real part and Z″ is the imaginary part of the impedance, respectively. The Nyquist plots consist of three characteristic regions. (1) A low-frequency region that is represented by an inclined line along the imaginary axis that shows capacitive behavior also known as the double-layer capacitive region. (2) A high-frequency region represented by a partial semicircle which shows the blocking behavior of the supercapacitor (in this region, the supercapacitor behaves as a pure resistor and the resistance values determine
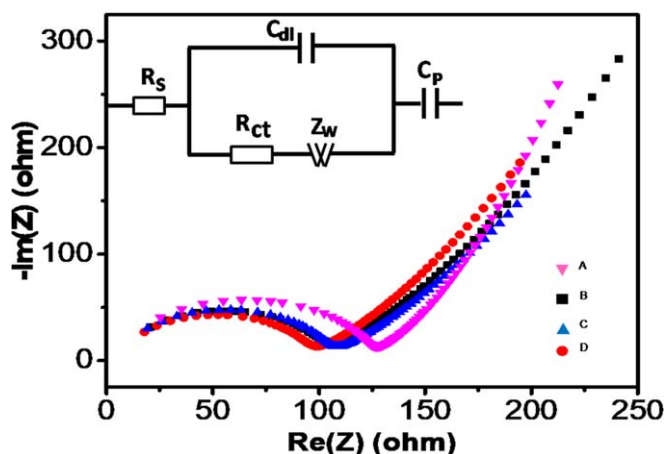
Figure 9. Nyquist plots for PVA and PVA/SF-SWNT nanocomposites. Generalized Randles equivalent circuit (in inset) is employed to model the charge transfer process. R_S is the solution resistance, R_{ct} is the charge transfer resistance and C_{dl} models the double layer capacitance, C_P is the pseudocapacitance and Z_W is the Warburg constant here. The values of the fitting parameters are shown in table 2.

Table 2. EIS fitting results for the electrodes with PVA (A) and PVA/SF-SWNTs (B, C, D) nanocomposite using the equivalent circuit from figure 9.

Sample	SF-SWNT concentration per gram (μl)	Equivalent series resistance R_s (Ω)	Electric double-layer capacitance C_{dl} (nF)	Charge-transfer resistance R_{ct} (Ω)	Pseudo-capacitance C_P (μF)
A	0	8.48	3.61	112.30	9.45
B	50	8.48	4.77	89.97	11.29
C	100	8.48	5.08	93.23	22.47
D	200	8.48	5.73	83.83	26.47

the charge-transfer and series resistance of the electrode). (3) A middle-frequency range that shows the effect of electrode thickness and the porosity on the diffusion of ions from an electrolyte to the electrode.

In order to evaluate the faradic process inside the device, its frequency based electrical behavior can be modeled as an AC equivalent circuit (generalized Randles circuit) [52]. The inset of figure 9 shows the equivalent circuit used for fitting the curve of the PVA/SF-SWNT nanocomposites. Here, R_s refers to the equivalent series resistance or the combined ohmic resistance of the electrolyte and the internal resistance of the electrode and current collectors. R_{ct} is the charge-transfer resistance during the faradic reaction, and is obtained from the diameter of the semicircle, illustrates the charge transfer resistance that occurs at the interface between the electrode and electrolyte. C_{dl} is the electric double-layer capacitance. Z_w is the Warburg impedance that represents the impedance of the diffusion controlling process in the electrolyte. The 45° region in the Nyquist plot is known as the Warburg region; the slope of this portion of the curve gives the value of Z_w. C_P is the pseudocapacitance, which can also be denoted by CPE, the constant-phase element. The semicircle impedance represents R_{ct} and Z_W. The semicircle in the high-frequency region corresponds to the charge transfer resistance at the electrode/electrolyte interface, while the linear relationship in the low-frequency region mainly represents pure capacitive behavior [43, 53]. The values of different components of the circuit obtained from the best fit of the experimental data using the equivalent circuit are reported in table 2.

The Nyquist plot clearly shows that in the high-frequency region, the samples had a series resistance value ($R_s = 8.48\ \Omega$). Moreover, the impedance spectrum of nanocomposite for sample D showed the smallest semicircle ($R_{ct} = 83.83\ \Omega$) than that of the other samples (for sample A, $R_{ct} = 112.30\ \Omega$). This suggests that sample D had a good electrical conductivity between the prepared electrode and current collecting electrode, as well as fast electron-conducting ability at the electrode surface, resulting in a significant increase in the capacitance value of sample D. The double-layer capacitance also increases with the amount of SWNTs in the composite and highest value was obtained for sampled D. Additionally, in the low-frequency region, vertical straight line implies an ideal capacitance with a higher rate of electrolyte diffusion and mass transfer. However, the straight lines of the electrodes have a slope of approximately 45° and there was no obvious change in the slope, indicating that the number of SWNTs did not significantly affect the diffusion of the ions [54].

4. Conclusions

In summary, PVA/SF-SWNT nanocomposites were synthesized by taking an ultralow concentration of SF-SWNT and their structural, surface morphological, thermal, electrical, mechanical, and electrochemical properties have been studied. SF-SWNT nanofiller improves the mechanical strength and DC electrical conductivity of the nanocomposite. The incorporation of SF-SWNT also enhances the specific capacitance of the nanocomposite. The enhancement of the specific capacitance of PVA/SF-SWNT nanocomposite can be attributed to the large surface area to volume ratio provided by the SWNT together with the absence of surfactant molecules that hindered the ions to come closer to the surface of the film. Considering the simplicity and effectiveness of the synthesis process, results indicate that the PVA/SF-SWNT nanocomposite may open up a low-cost route for the synthesis of flexible energy storage applications.

Acknowledgments

ORCID iDs

Muhammad Rakibul Islam ⓘ https://orcid.org/0000-0003-3931-3066
Saiful I Khondaker ⓘ https://orcid.org/0000-0003-1333-1928

References

[1] Kuilla T *et al* 2010 Recent advances in graphene based polymer composites *Prog. Polym. Sci.* **35** 1350–75
[2] Kim D J, Jo M J and Nam S Y 2015 A review of polymer–nanocomposite electrolyte membranes for fuel cell application *J. Ind. Eng. Chem.* **21** 36–52
[3] Hanemann T and Szabó D V 2010 Polymer-nanoparticle composites: from synthesis to modern applications *Materials.* **3** 3468–517
[4] Hosseini S F *et al* 2015 Fabrication of bio-nanocomposite films based on fish gelatin reinforced with chitosan nanoparticles *Food Hydrocoll.* **44** 172–82
[5] Merino S *et al* 2015 Nanocomposite hydrogels: 3D polymer–nanoparticle synergies for on-demand drug delivery *ACS Nano.* **9** 4686–97
[6] Kim H, Abdala A A and Macosko C W 2010 Graphene/polymer nanocomposites *Macromolecules* **43** 6515–30
[7] Sahoo S *et al* 2013 Graphene/polypyrrole nanofiber nanocomposite as electrode material for electrochemical supercapacitor *Polymer* **54** 1033–42
[8] Zeng C *et al* 2010 Synthesis and processing of PMMA carbon nanotube nanocomposite foams *Polymer* **51** 655–64
[9] Sundaray B *et al* 2006 Electrical conductivity of a single electrospun fiber of poly(methyl methacrylate) and multiwalled carbon nanotube nanocomposite *Appl. Phys. Lett.* **88** 143114
[10] Cao X *et al* 2009 The enhanced mechanical properties of a covalently bound chitosan-multiwalled carbon nanotube nanocomposite *J. Appl. Polym. Sci.* **113** 466–72
[11] Yun S I *et al* 2008 Mechanical properties of biodegradable polyhydroxyal kanoates/single wall carbon nanotube nanocomposite films *Polym. Bull.* **61** 267–75
[12] Laird E D and Li C Y 2013 Structure and morphology control in crystalline polymer–carbon nanotube nanocomposites *Macromolecules* **46** 2877–91
[13] Ghai V, Baranwal A, Singh H and Agnihotri P K 2019 Design and fabrication of a multifunctional flexible absorber (flexorb) in the UV–Vis–NIR wavelength range *Adv. Mater. Technol.* **4** 1900513
[14] Ghai V, Singh H and Agnihotri P K 2020 Near perfect thin film flexible broadband optical absorber with high thermal/electrical conductivity *J. Appl. Polym. Sci.* **137** 48855
[15] Grady B P 2010 Recent developments concerning the dispersion of carbon nanotubes in polymers *Macromol. Rapid Commun.* **31** 247–57
[16] Mu M and Winey K I 2007 Improved load transfer in nanotube/polymer composites with increased polymer molecular weight *J. Phys. Chem.* C **111** 17923–7
[17] Gong X *et al* 2000 Surfactant-assisted processing of carbon nanotube/polymer composites *Chem. Mater.* **12** 1049–52
[18] Carter R *et al* 2014 Solution assembled single walled carbon nanotube foams; superior performance in supercapacitors *J. Phys. Chem.* C **118** 20137–51
[19] Islam M R and Khondaker S I 2014 Recent progress in parallel fabrication of individual single walled carbon nanotube devices using dielectrophoresis *Mater. Express* **4** 263–78
[20] Stokes P and Khondaker S I 2010 Evaluating defects in solution processed carbon nanotube devices via low temperature transport spectroscopy *ACS Nano.* **4** 2659–66
[21] Stokes P and Khondaker S I 2010 High quality solution processed carbon nanotube transistors assembled by AC dielectrophoresis *Appl. Phys. Lett.* **96** 083110
[22] Ling Y *et al* 2013 A printable cnt-based fm passive wireless sensor tag on a flexible substrate with enhanced sensitivity *IEEE Sens. J.* **14** 1193–7
[23] Ervin M H *et al* 2012 A comparison of single-wall carbon nanotube electrochemical capacitor electrode fabrication methods *Electrochim. Acta* **65** 37–43
[24] Aslam M, Kalyar M A and Raza Z A 2018 Polyvinyl alcohol: a review of research status and use of polyvinyl alcohol based nanocomposites *Polym. Eng. Sci.* **58** 2119–32

[25] Shekhar S, Stokes P and Khondaker S I 2011 Ultra-high density alignment of carbon nanotubes array by dielectrophoresis *ACS Nano* **5** 1739–46

[26] Bai Q *et al* 2015 Thermal and water dual-responsive shape memory poly(vinyl alcohol)/Al$_2$O$_3$ nanocomposite *RSC Adv.* **5** 91213–7

[27] Mallakpour S and Ezhieh A N 2017 Preparation and characterization of chitosan-poly(vinyl alcohol) nanocomposite films embedded with functionalized multi-walled carbon nanotube *Carbohydr. Polym.* **166** 377–86

[28] Kumar K N *et al* 2017 Bright green emission from f-MWCNT embedded co-doped Bi$_3^+$ Tb$_3^+$: polyvinyl alcohol polymer nanocomposites for photonic applications *RSC Adv.* **7** 15084–95

[29] Alghunaim N S 2016 Optimization and spectroscopic studies on carbon nanotubes/PVA nanocomposites *Results Phys.* **6** 456–60

[30] Doudou B B *et al* 2014 Hybrid carbon nanotube—silica/polyvinyl alcohol nanocomposites films: preparation and characterization *J. Polym. Res.* **21** 420

[31] Paiva M C *et al* 2014 Mechanical and morphological characterization of polymer–carbon nanocomposites from functionalized carbon nanotubes *Carbon* **42** 2849–54

[32] Bhavani S *et al* 2013 Structural and electrical properties of pure and NiCl$_2$ doped PVA polymer electrolytes *American Journal of Polymer Science* **3** 56–62

[33] Cadek M *et al* 2002 Morphological and mechanical properties of carbon-nanotube-reinforced semicrystalline and amorphous polymer composites *Appl. Phys. Lett.* **81** 5123–5

[34] Liu L *et al* 2005 Mechanical properties of functionalized single-walled carbon-nanotube/poly(vinyl alcohol) nanocomposites *Adv. Funct. Mater.* **15** 975–80

[35] Cadek M *et al* 2004 Reinforcement of polymers with carbon nanotubes: the role of nanotube surface area *Nano Lett.* **4** 353–6

[36] Prasada K E *et al* 2009 Extraordinary synergy in the mechanical properties of polymer matrix composites reinforced with 2 nanocarbons *Proc. Natl Acad. Sci.* **106** 13186–9

[37] van der Pauw L J 1958 A method of measuring the resistivity and hall coefficient on lamellae of arbitrary shape *Philips Tech. Rev.* **20** 220–4

[38] Hosein A, Hoseini A, Arjm M, Sundararaj U and Trifkovic M 2017 Significance of interfacial interaction and agglomerates on electrical properties of polymer-carbon nanotube nanocomposites *Mater. Des.* **125** 126–34

[39] Gardea F and Lagoudas D C 2014 Characterization of electrical and thermal properties of carbon nanotube/epoxy composites *Compos Part B: Eng.* **56** 611–20

[40] Tsai Y C and Huang J D 2006 Poly (vinyl alcohol)-assisted dispersion of multiwalled carbon nanotubes in aqueous solution for electroanalysis *Electrochem. Commun.* **8** 956–60

[41] Liu D *et al* 2011 Fabrication and characterization of zirconium hydroxide- carboxymethyl cellulose sodium/plasticized Trichosanthes Kirilowii starch nano-composites *Carbohydr. Polym.* **86** 1699–704

[42] G Zhengyang *et al* 2020 One-Step Electrofabrication of Reduced Graphene Oxide/Poly(N-methylthionine) Composite Film for High Performance Supercapacitors *J. Electrochem. Soc.* **167** 085501

[43] Bao S J *et al* 2008 Biomolecule-assisted synthesis of cobalt sulfide nanowires for application in supercapacitors *J. Power Sources* **180** 676–81

[44] Lehtimäki S *et al* 2014 Low-cost, solution processable carbon nanotube nanocomposite supercapacitors and their characterization *Appl. Phys. A* **117** 1329–34

[45] Kaempgen M *et al* 2009 Printable thin film supercapacitors using single-walled carbon nanotubes *Nano Lett.* **9** 1872–6

[46] Hu S, Rajamani R and Yu X 2012 Flexible solid-state paper based carbon nanotube supercapacitor *Appl. Phys. Lett.* **100** 104103

[47] Koysuren O 2012 Preparation and characterization of polyvinyl alcohol/carbon nanotube (PVA/CNT) conductive nanofibers *J. Polym. Eng.* **32** 407–13

[48] Peng C, Zhang S, Jewell D and Chen G Z 2008 Carbon nanotube and conducting polymer composites for supercapacitors *Prog. Nat. Sci.* **18** 777–88

[49] Zhang D *et al* 2012 Enhanced capacitive deionization performance of graphene/carbon nanotube composites *J. Mater. Chem.* **22** 14696–704

[50] Zhou Y-K *et al* 2004 Electrochemical capacitance of well-coated single-walled carbon nanotube with polyaniline composites *Electrochim. Acta* **49** 257–62

[51] Wu Z S, Parvez K, Feng X and Mu¨llen K 2013 Graphene-based in-plane micro-supercapacitors with high power and energy densities *Nat. Commun.* **4** 2487

[52] Vyas R N, Li K and Wang B 2010 Modifying randles circuit for analysis of polyoxometalate layer-by-layer films *J. Phys. Chem.* B **114** 15818–24

[53] Li Q, Zhu Y Q and Eichhorn S J 2018 Structural supercapacitors using a solid resin electrolyte with carbonized electrospun cellulose/carbon nanotube electrodes *J. Mater. Sci.* **53** 14598–607

[54] Gilshteyn E P *et al* 2018 Flexible self-poweredpiezo-supercapacitor system forwearable electronics *Nanotechnology* **29** 325501